Ground Motion Attenuation during M7.1 Darfield and M6.3 Christchurch (New Zealand) Earthquakes and Performance of Global Predictive Models

Margaret Segou (U.S. Geological Survey, Menlo Park, CA)
Erol Kalkan (U.S. Geological Survey, Menlo Park, CA)

Introduction

M7.1 Darfield earthquake occurred 40 km west of Christchurch (New Zealand) on September 4th 2010. Six months after, the city was struck again with a M6.3 event on February 21st. These events resulted in significant damage to city's infrastructure and its suburbs. The purpose of this study is to evaluate the performance of global predictive models using the strong motion data obtained from these two events to improve future seismic hazard assessment and building code provisions for the Canterbury region.

The Canterbury region is located on the boundary between the Pacific and Australian plates; its surface expression is the active right lateral Alpine Fault (Berryman et al., 1993). Beneath the North Island and the north South Island, the Pacific plate subducts obliquely under the Australian plate, while at the south-western part of South Island, a reverse process takes place. Although New Zealand has experienced several major earthquakes in the past as a result of its complex seismotectonic environment (e.g., M7.1 1888 North Canterbury, M7.0 1929 Arthur's Pass and M6.2 1995 Cass), there was no evidence of prior seismic activity in Christchurch and its surroundings before the September event. The Darfield and Christchurch earthquakes occurred in the previously unmapped Greendale Fault in the Canterbury basin, covered by Quaternary alluvial deposits (Forsyth et al., 2008). In Figure 1, site conditions of the Canterbury epicentral area is depicted on a V_{S30} map. This map was determined on the basis of topographic slope calculated from a 1-km grid using the method of Allen and Wald (2007). Also shown are the locations of strong motion stations.

The Darfield event was generated as a result of a complex rupture mechanism; the recordings and geodetic data reveal that earthquake consists of three sub-events (Barnhart et al., this issue). The first event was due to rupturing of a blind reverse fault with M6.2, followed by a second event (M6.9), releasing the largest portion of the energy on the right-lateral Greendale fault. The third sub-event (M5.7) is due to a reverse fault with a right-lateral component (Holden et al., 2011). The Christchurch earthquake, however, occurred on an oblique thrust fault. The comparison of spectral acceleration values at stations near Christchurch reveals that later event produced much larger amplitudes of shaking than the Darfield event due to its proximity to the epicenter. Both events resulted in noticeably large amplitudes of the vertical motion, exceeding horizontal motion in the near fault area. The vertical motions, showing asymmetric acceleration traces and pulses, reached 1.26 g during the Darfield, and 2.2 g during the Christchurch event. These events were recorded by more than 100 strong motion stations operated by the Institute of Geological and Nuclear Sciences (http://www.geonet.org.nz/). Using the processed data from these stations, peak ground

acceleration (PGA), and 5%-damped spectral acceleration values at 0.3, 1, and 3 s are used for performance evaluation of the global ground motion predictive equations (GMPEs). The selected GMPEs are the Next Generation Attenuation (NGA) models of Abrahamson and Silva (2008), Boore and Atkinson (2008), Campbell and Bozorgnia (2008), and Chiou and Youngs (2008). Graizer and Kalkan (2007 and 2009) model, which is based on the NGA project database, is also included. These GMPEs are abbreviated respectively as AS08, BA08, CB08, CY08 and GK07. Because they have been used widely for seismic hazard analysis for shallow crustal regions, their performance assessment becomes a critical issue especially for immediate response and recovery planning after major events. It is expected that aftershocks similar to Christchurch will control the seismic hazard in the area as confirmed by the recent M6.0 event on June 13th.

Performance Evaluation of Ground Motion Prediction Equations

In order to evaluate the relative performance of the GMPEs and their ranking to be used for logic tree weighting in hazard analysis, we used traditional residual analysis and an information theoretic approach. In residual analysis the prediction error for each observation and standard deviation of the errors for each event are computed for each GMPE. Residuals correspond to the difference between the observations and predictions in natural-log space; negative residuals are interpreted as overprediction, whereas positive residuals indicate underestimation of the predictive model. The applied information theoretic approach is based on a log-likelihood value (LLH), which describes the information loss when a GMPE approximates an observation (Scherbaum et al. 2009). The average sample log-likelihood (LLH) value of a GMPE over *N* observations, represented by a log-normal distribution, is calculated as:

$$log\big(L(g|x)\big) = -\frac{1}{N}\sum_{i=1}^{N} log\big(g(x_i)\big) \qquad (1)$$

The negative average log-likelihood value is a measure of distance between the predictions and observations; therefore, a GMPE exhibiting a smaller absolute value of LLH, relative to other GMPEs, corresponds to a better performing model.

For the Darfield event, the relative performance of GMPEs was evaluated for strike slip faulting since the greater amount of moment release occurred during the second sub-event. For the Christchurch event, however, the evaluation is based on the thrust fault (as discussed before). The hanging wall effects were considered although their effects are not significant because the causative faults appear to be steep (Bradley and Cubrinovski, this issue). The flat-file, listing distance metrics, V_{S30} for each station, and corresponding observations (PGA and spectral values), is provided for each event as an electronic supplement (http://nsmp.wr.usgs.gov/ekalkan/NZ/index.html). Using this flat-file, predictions of GMPEs were computed for each event. Figures 2-5 summarize the results for the M7.1 Darfield (top panels) and M6.3 Christchurch (bottom panels) earthquakes. The plots shown in row-A in each figure represent

16, 50 (median) and 84 percentile of predictions considering an average V_{S30} value of 400 m/s. In these plots, observations correspond to the maximum value of two horizontal components. Because the NGA models predict geometric mean of ground motion, their predictions were adjusted for maximum horizontal component by multiplying their predictions with 1.1, 1.15 and 1.18 and 1.18 respectively for PGA, spectral acceleration at 0.3 s, 1 s, and 3 s. These adjustment factors were adapted from Campbell and Bozorgnia (2008). The GK07 model predicts the maximum of the two horizontal components. It should be also noted that both observations and predictions are plotted against the distance metric, specific to the model; for the BA08, the distance metric is the "Joyner-Boore distance" (R_{JB}), defined as the closest distance from the recording station to the surface projection of the fault rupture plane (Boore et al., 1997). For the remaining models, the distance measure is the "closest fault distance" (R_{rup}) defined as the closest distance to co-seismic rupture plane.

The next set of plots in Figures 2-5 (row-B) show the distance distribution of residuals. Linear fit lines illustrates the distance bias; the trend line passing through zero means that there is no bias in predictions. Unlike the attenuation curves shown in row-A, based on average V_{S30}, the residuals are computed based on specific V_{S30} values at each station estimated from topographic slope (Fig. 1) in order to explicitly incorporate the site effects on ground motion estimates. To quantify the quality of fit, the standard errors of predictions (σ_{lnY}) are computed based on residuals, and these values are given in each panel for each GMPE. The larger σ_{lnY} indicates a poorer performance of the GMPE. For PGA, all GMPEs indicate an overall good fit to observations up to ~100 km (Fig. 1 row-A); for distances larger than 100 km, ground motion exhibits faster attenuation, as a result the observed peak values are lower than expected. This is more pronounced for the Christchurch event. Low ground accelerations recorded at large distances show the effect of the anelastic attenuation due to regional low Q (Zhao and Gerstenberger, 2010).

In Figure 2 (row-B), residuals for the Darfield event reveal overestimation for distances greater than 70 km for the AB08 and 100 km for the BA08 and CB08 models. On the other hand, the GK07 and CY08 fit better to the observations because their trend lines fitting to residuals do not show a notable distance bias. For the AS08 and CB08, the misfit at larger distances is more evident. In case of PGA, the GK07, BA08 and CY08 models yield the smallest σ_{lnY} of 0.52 for the Darfield event. For the Christchurch event (Fig. 2 bottom panels), the GK07, AS08, BA08 and CY08 present better residual fits than CB08 for which the overestimation begins at 20 km. The smallest σ_{lnY} is due to the CY08. The same is true for spectral acceleration at 0.3 s as shown in Figure 3 (row-B). Finally, Figure 2 (row-C) shows the distance distribution of LLH values. In these plots, trend lines identify the consistency of the GMPE in predicting ground motion at various distances; if the slope is close to zero, then GMPE has low distance variability, meaning that it is consistent. Much higher LLH values with increasing distance suggest a poorer fit at far-field, which is observed for all GMPEs for the Christchurch event.

As shown in Figure 3, spectral acceleration at 0.3 s reaches 1 g at 40 km for the Darfield, and 2 g at 10 km for the Christchurch earthquake. For the Darfield event, the AS08 and CB08 overestimate observations for distances

larger than 70 km as shown by the residual plots. The same trend is evident for the Christchurch event (Fig. 3 bottom panels). The BA08 performs better for the Darfield event since there is only a minor overestimation for distances larger than 20 km. For the Christchurch event (Fig. 3 bottom panels), however, the distance trend line of LLH reveals a poorer performance of the BA08 and CB08.

Ground motion estimates are given for spectral acceleration at 1 s in Figure 4, where the observations exceed 1 g in the near field of both earthquakes. For Darfield, all GMPEs present an excellent fit to the observations up to 70 km from the fault. Beyond 70 km, they slightly overestimate the observations due to faster attenuation of ground motion at far distances. For the Christchurch event, the overestimation is evident for the BA08 and CB08 over 50 km, which resulted in higher LLH values.

In Figure 5 (top panels), comparisons are given for the spectral acceleration at 3 s. For both Darfield and Christchurch events, spectral peaks reach 0.5 g. For the former event, the GK07 is the best fitting model to observations with zero distance bias and with lowest LLH values. The NGA models underestimate long period ground motions up to 100 km, whereas beyond 100 km they tend to overestimate. For the Christchurch earthquake, none of the models provide an excellent fit (Fig. 4 bottom panels). The GK07 overestimates observations, as opposed to underestimation of NGA models over a wide distance range.

Ranking Ground Motion Prediction Equations

In Table 1, the mean ($\boldsymbol{\mu_{LLH}}$) and standard deviation ($\boldsymbol{\sigma_{LLH}}$) of LLH values over the total number of observations for each earthquake and for each GMPE are tabulated, the standard errors ($\sigma_{\ln Y}$) of predictions are also listed. This table is used for ranking the GMPEs according to these three parameters. For ranking, each parameter is first normalized with the respect to its lowest value due to different GMPEs, and then the arithmetic-mean of normalized values is computed for $\boldsymbol{\mu_{LLH}}$, $\boldsymbol{\sigma_{LLH}}$, and $\sigma_{\ln Y}$ for each GMPE. The GMPE with the lowest arithmetic-mean is ranked as first. This exercise is repeated for each period and for each earthquake, and the results of ranking are given in Table 2. The best performing GMPE has a combined performance value close to unity. The ranking results show that performance of the GK07, BA08 and CY08 are equally the same for different periods and events, while the CB08 and AS08 show relatively poorer performance.

Concluding Remarks

In this study, performance of global ground motion prediction equations (GMPEs) was examined for the New Zealand M7.1 Darfield and M6.3 Christchurch earthquakes, with the objective of improving future seismic hazard assessment and engineering applications for the Canterbury region. These events are characterized by producing significantly large ground motions at high frequencies, which showed faster attenuation through the crust due to low regional Q. Amplified spectral accelerations at long periods at long distances are attributed to Canterbury's deep sedimentary basin. For similar shallow earthquakes in New Zealand, there is an evidence of Moho reflection, which might be

potentially amplified long periods ground motions further (Zhao and Gerstenberger, 2010). Comparison of predictions derived from the five different GMPEs with observations reveal overall good performance of these models supporting their applicability for the region. For the purpose of selecting and weighting GMPEs in a logic tree approach for regional seismic hazard analysis, we applied a simple ranking procedure based on the average LLH values considering their mean and standard deviation, as well as standard errors (σ_{lnY}) of predictions. The ranking results show that performance of GK07 (Graizer and Kalkan, 2007, 2009), BA08 (Boore and Atkinson, 2008) and CY08 (Chiou and Youngs, 2008) are equally the same, while the CB08 (Campbell and Bozorgnia, 2008) and AS08 (Abrahamson and Silva, 2008) show relatively poorer performance.

Acknowledgements

The authors thank Jim Cousins (GNZ) for providing parameters of strong motion recordings, and Volkan Sevilgen for preparing the V_{S30} map for the Canterbury region. We also wish to thank David Boore and Paul Spudich for their reviews.

Data and Resources

For NGA models, we used the Fortran code written by David Boore; for Graizer and Kalkan (2007, 2009) ground motion prediction model, Matlab and Fortran codes are available online at http://nsmp.wr.usgs.gov/ekalkan/PGA07/index.html. The flat-file for both Darfield and Christchurch events are also available online at http://nsmp.wr.usgs.gov/ekalkan/NZ/index.html.

References

Abrahamson, N. A. and W. J. Silva (2008). Summary of the Abrahamson and Silva NGA ground motion relations. Earthquake Spectra 24 (1), 67–98.

Allen, T. I., and Wald, D. J. (2007). Topographic Slope as a Proxy for Seismic Site Conditions (V_s^{30}) and Amplification around the Globe, U.S. Geological Survey, Open File Report 2007-1357, 69 pp.

Barnhart, W., Willis, M.J., Lohman, R. W., Melkonian, A. (2011). InSAR and optical constraints on fault slip during the 2010-2011 New Zealand earthquake sequence, this issue.

Berryman , K.R., Beanland, S. Cooper, A. F., Cutten, H. N., Norris, R. J. and Wood, P. R. (1993). The Aplpine fault, new Zealand: Variation in Quaternary structural style and geomorphic expression, Annales Tectonicae, Special issue-supplement to v. 6, 126-163.

Boore, D. M. Joyner, W. B. and Fumal, T. E. (1997). Equations for estimating horizontal response spectra and peak acceleration from western North American earthquakes: a summary of recent work, Seismol. Res. Lett. Vol. 68, pp. 128-153.

Boore, D. M. and Atkinson, G. M. (2008). Ground motion prediction equations for the average horizontal component of PGA, PGV, and 5%-damped PSA at spectral periods between 0.01 s and 10.0 s, Earthquake Spectra, Vol. 24, No. 1, pp. 99-138.

Bradley B.A. and Cubrinovski, M. (2011). Near field strong ground motions observed in the 22 February 2011 Cristchurch earthquake, this issue.

Campbell, K. W. and Bozorgnia, Y. (2008). NGA ground motion model for the geometric mean horizontal component of PGA, PGV, PGD and 5% damped linear elastic response spectra for periods ranging from 0.01 to 10 s, Earthquake Spectra, Vol. 24, No. 1, pp. 139-172.

Chiou B. S. J, Youngs. R. R. (2008). An NGA Model for the Average Horizontal Component of Peak Ground Motion and Response Spectra, Earthquake Spectra, Vol. 24, No. 1, pp. 173-215.

Forsyth, P. J., Barrell, D. J. A. and Jongens, R. (2008). Geology of the Christchurch Area. Institude of Geological and Nuclear Sciences 1;250 000 geological map 16, 1 sheet + 67 pp. Lower Hutt, NZ, GNS Science.

Graizer, V. and Kalkan, E. (2007). Ground motion attenuation model for peak horizontal acceleration from shallow crustal earthquakes, Earthquake Spectra, Vol. 23, pp. 585–613.

Graizer V. Kalkan E. (2009). “Prediction of Response Spectral Acceleration Ordinates based on PGA Attenuation”, Earthquake Spectra, Vol. 25, No. 1, pp. 36 – 69.

Holden, C., Beavan, B., Fry, B., Reyners, M., Ristau, J., Van Dissen, R., Villamor, P. and Quigley, M. (2011). Preliminary source model of the Mw 7.1 Darfield earthquake from geological, geodetic and seismic data, Proceedings of the Ninth Pacific Conference on Earthquake Engineering Building an Earthquake-Resilient Society 14-16 April, 2011, Auckland, New Zealand, Paper Number 164.

Scherbaum, F., Delavaud, E. and Riggelsen, C., 2009. Model selection in seismic hazard analysis: An information-theoretic perspective, Bulletin of Seismological Society of America 99, 3234–3247.

Zhao, J. X. and Gerstenberger, M. (2010). Comparison of attenuation characteristics between the data from two distant regions, Proceedings of the Ninth Pacific Conference on Earthquake Engineering Building an Earthquake-Resilient Society 14-16 April, 2011, Auckland, New Zealand, Paper Number 008.

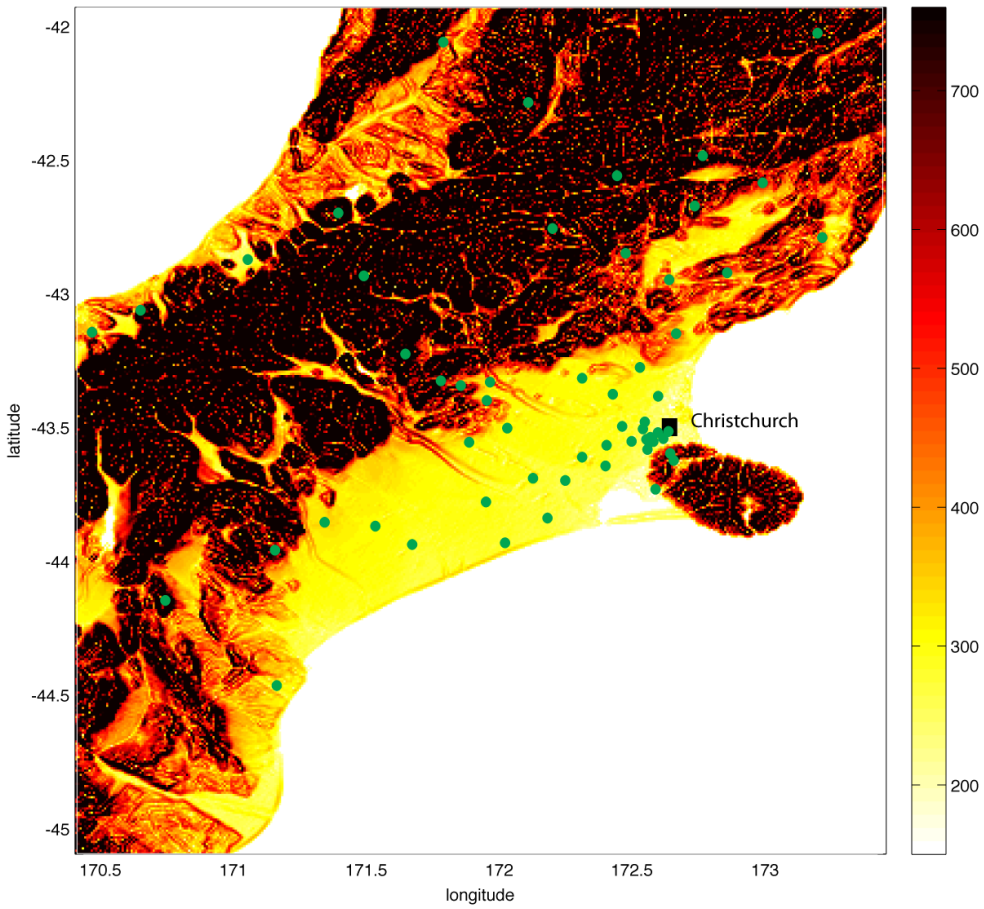

Figure 1. Shear-wave velocity (unit = m/s) down to 30 m derived from topographic slope; also shown are the location of strong motion stations.

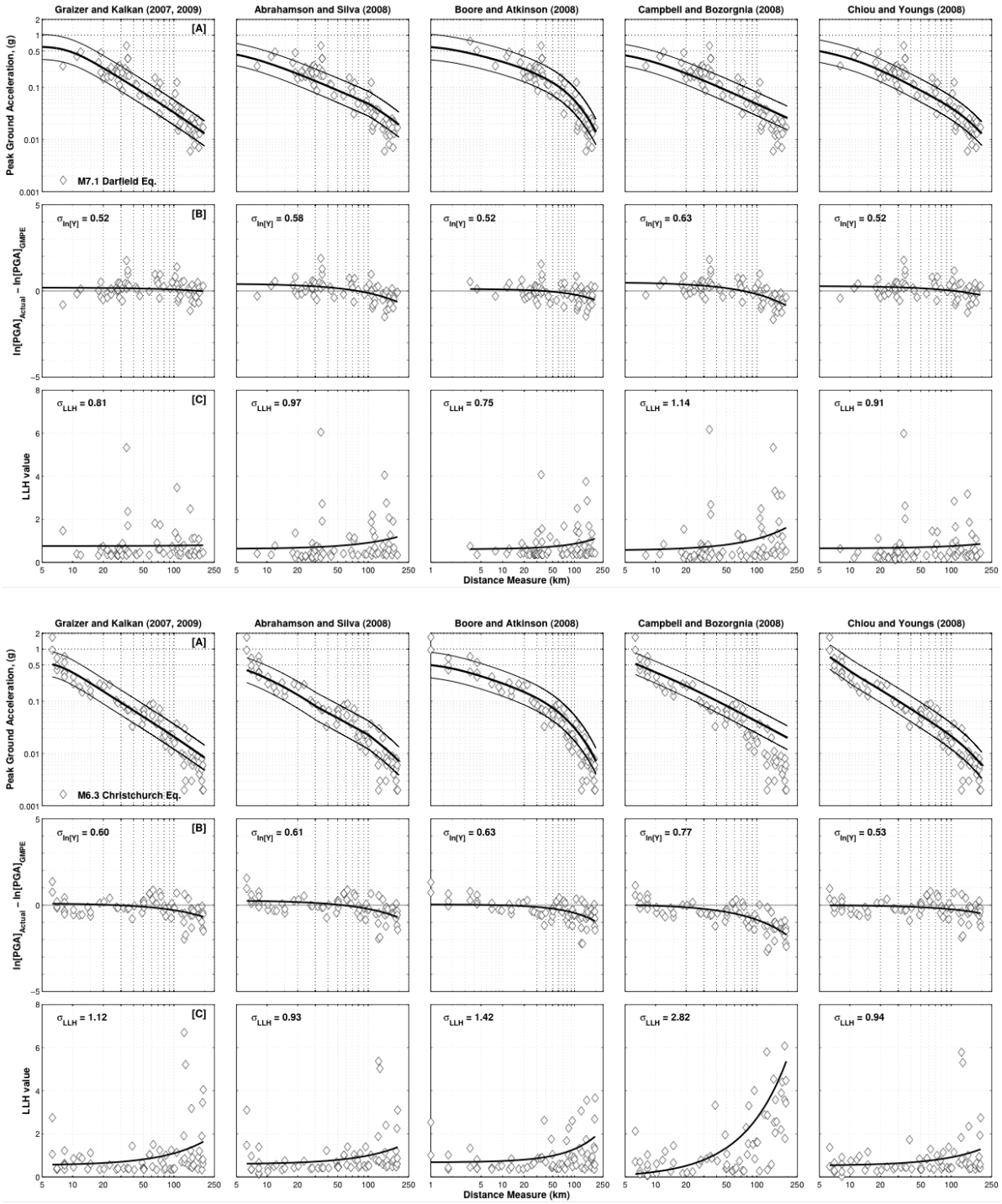

Figure 2. [A] Comparison of PGA values recorded from the M7.1 Darfield [top panels] and M6.3 Christchurch [bottom panels] earthquakes for 16, 50 (median) and 84 percentile predictions from five different GMPEs. [B] Residuals computed for each GMPE for median prediction; also shown is the trend line to quantify distance bias. [C] Average-log likelihood (LLH) values are to determine performance of GMPEs; higher LLH values indicate poorer performance.

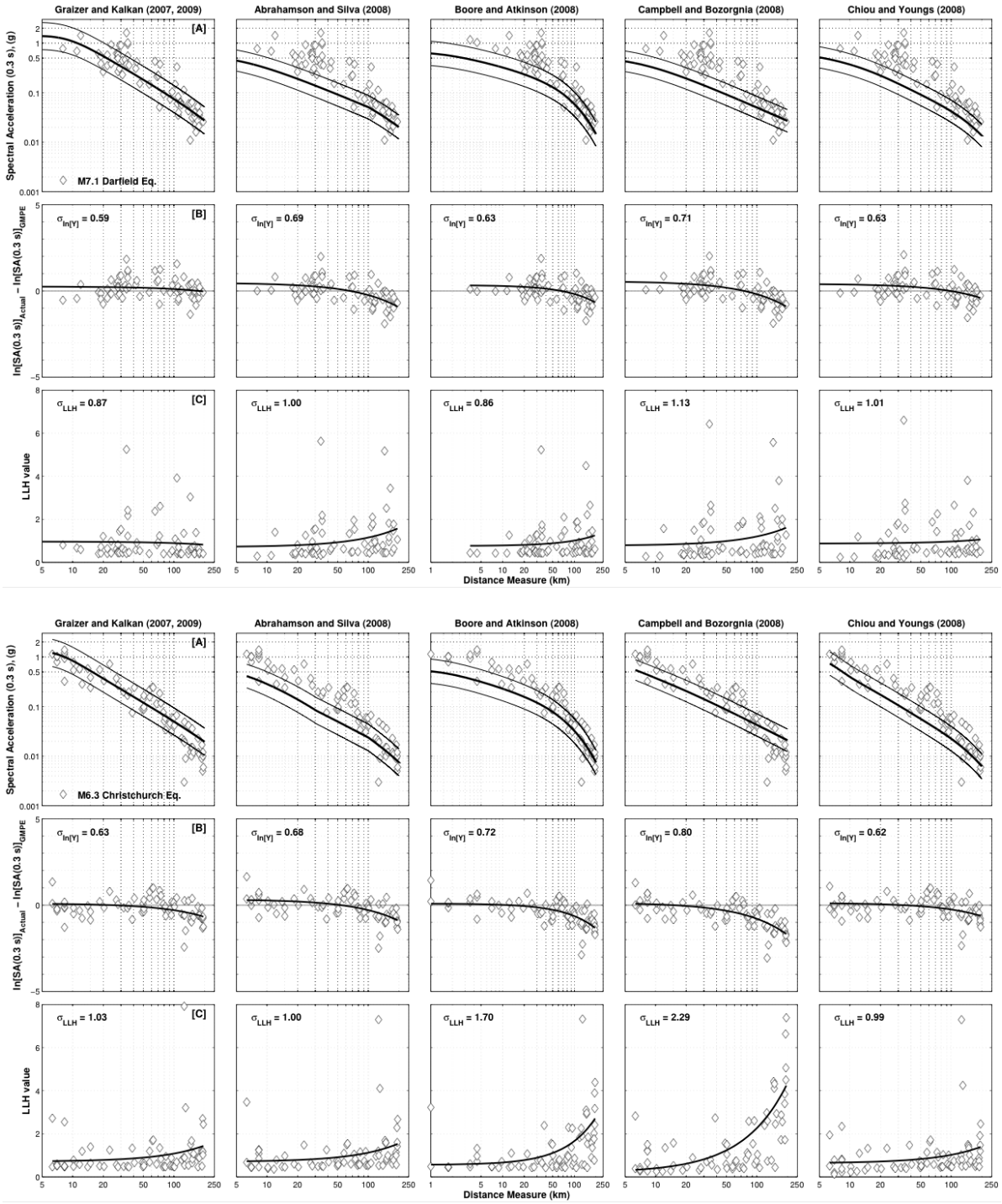

Figure 3. [A] Comparison of 5%-damped spectral acceleration values computed at 0.3 s for the M7.1 Darfield [top panels] and M6.3 Christchurch [bottom panels] earthquakes for 16, 50 (median) and 84 percentile predictions from five different GMPEs. [B] Residuals computed for each GMPE for median prediction; also shown is the trend line to quantify distance bias. [C] Average-log likelihood (LLH) values are to determine performance of GMPEs; higher LLH values indicate poorer performance.

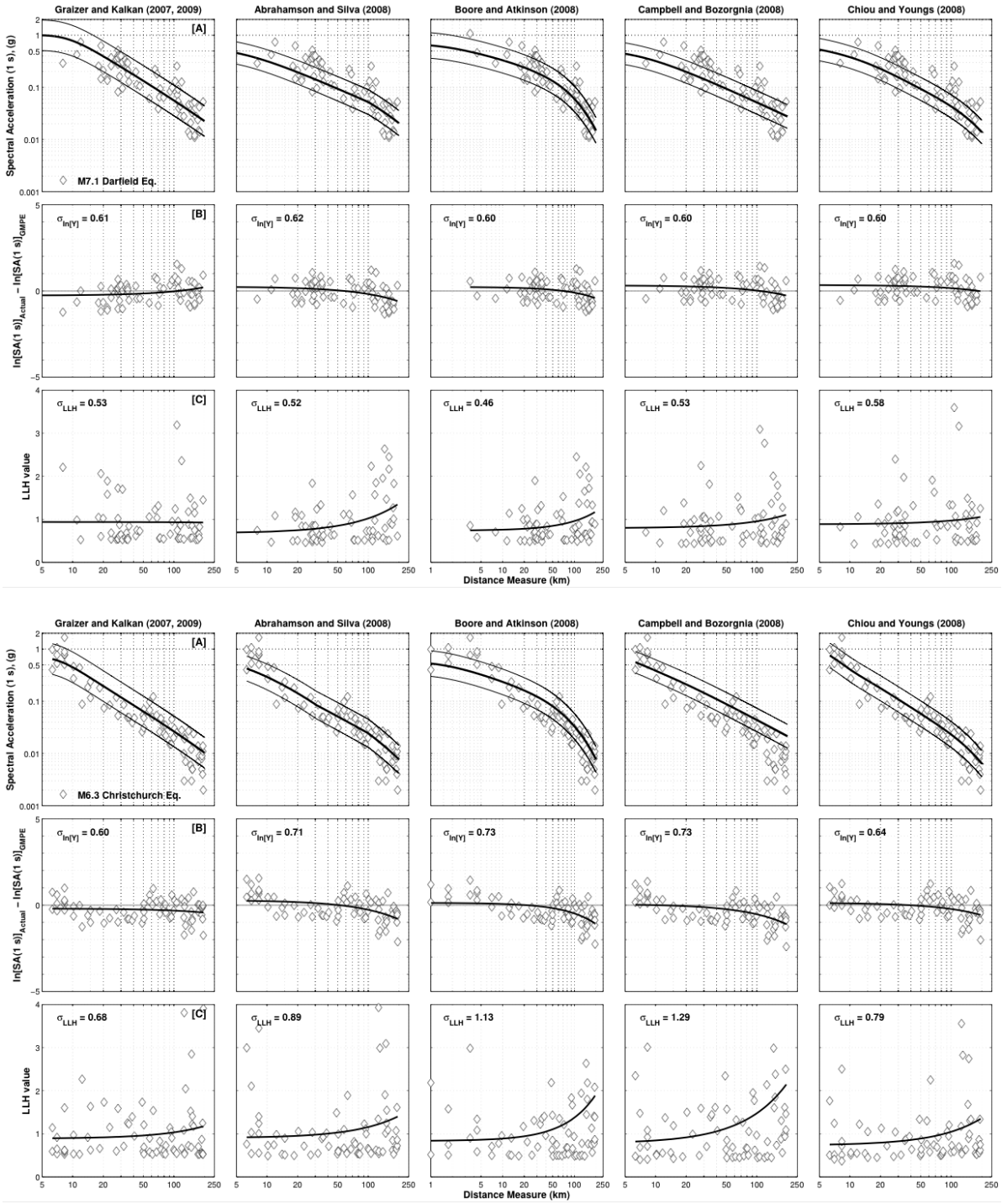

Figure 4. [A] Comparison of 5%-damped spectral acceleration values computed at 1 s for the M7.1 Darfield [top panels] and M6.3 Christchurch [bottom panels] earthquakes for 16, 50 (median) and 84 percentile predictions from five different GMPEs. [B] Residuals computed for each GMPE for median prediction; also shown is the trend line to quantify distance bias. [C] Average-log likelihood (LLH) values are to determine performance of GMPEs; higher LLH values indicate poorer performance.

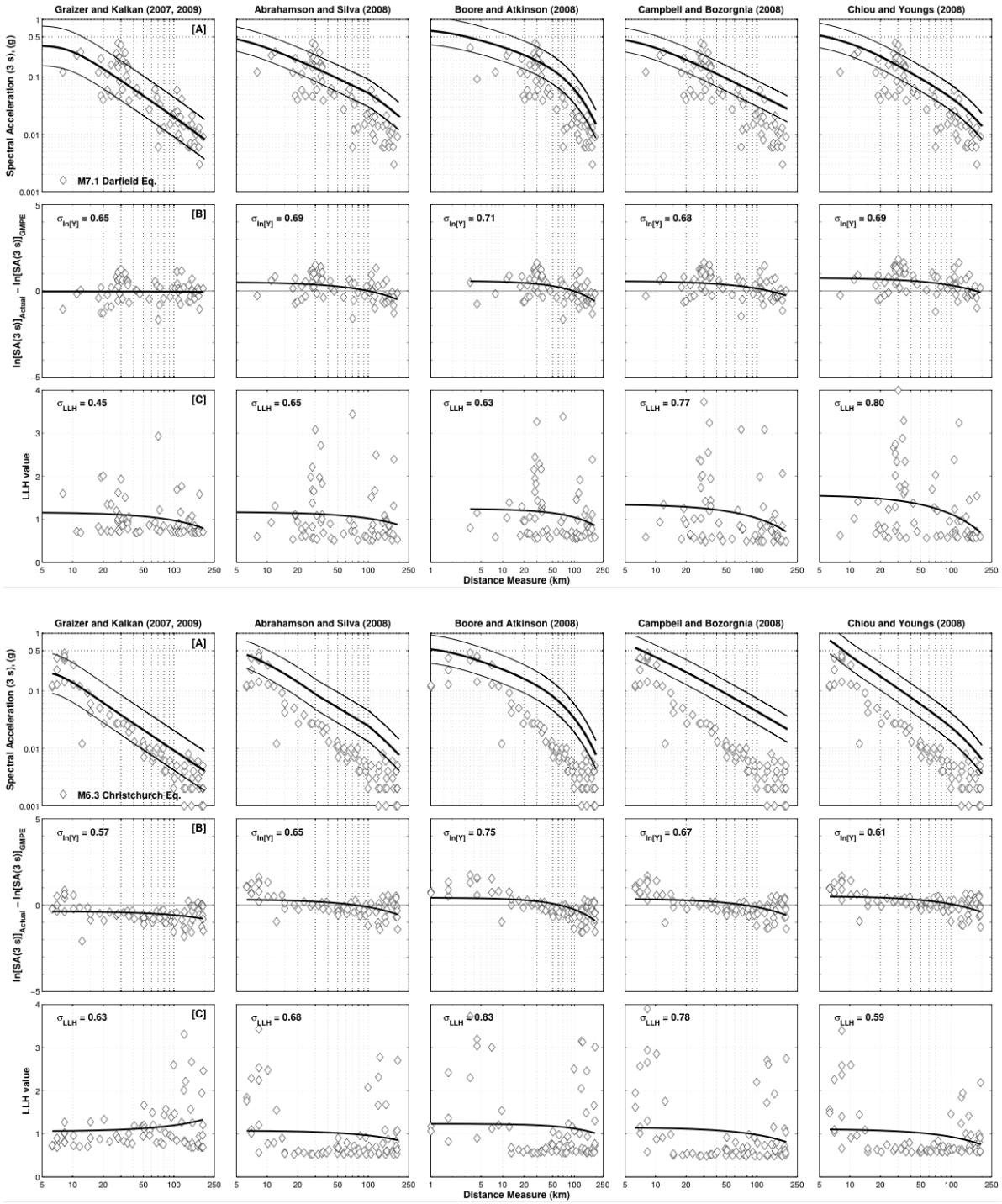

Figure 5. [A] Comparison of 5%-damped spectral acceleration values computed at 3 s for the M7.1 Darfield [top panels] and M6.3 Christchurch [bottom panels] earthquakes for 16, 50 (median) and 84 percentile predictions from five different GMPEs. [B] Residuals computed for each GMPE for median prediction; also shown is the trend line to quantify distance bias. [C] Average-log likelihood (LLH) values are to determine performance of GMPEs; higher LLH values indicate poorer performance.

Table 1. Mean (μ_{LLH}) and standard deviation (σ_{LLH}) of average log-likelihood (LLH) values, and standard error of predictions (σ_{lnY}). GK07: Graizer and Kalkan (2007 and 2009); AS08: Abrahamson and Silva (2008); BA08: Boore and Atkinson (2008); CB08: Campbell and Bozorgnia (2008); CY08: Chiou and Youngs (2008).

M7.1 Darfield	μ_{LLH}					σ_{LLH}					σ_{lnY}				
	GK07	**AS08**	**BA08**	**CB08**	**CY08**	**GK07**	**AS08**	**BA08**	**CB08**	**CY08**	**GK07**	**AS08**	**BA08**	**CB08**	**CY08**
PGA	0.77	0.84	0.80	0.96	0.73	0.80	0.96	0.74	1.13	0.90	0.52	0.58	0.52	0.63	0.52
SA (0.3s)	0.91	1.04	0.95	1.10	0.94	0.86	0.99	0.85	1.12	1.00	0.59	0.69	0.63	0.71	0.63
SA (1 s)	0.93	0.93	0.90	0.91	0.95	0.52	0.52	0.46	0.53	0.58	0.61	0.62	0.60	0.60	0.60
SA (3 s)	1.02	1.06	1.09	1.11	1.23	0.45	0.65	0.63	0.76	0.80	0.65	0.69	0.71	0.68	0.69
M6.3 Christchurch	μ_{LLH}					σ_{LLH}					σ_{lnY}				
	GK07	**AS08**	**BA08**	**CB08**	**CY08**	**GK07**	**AS08**	**BA08**	**CB08**	**CY08**	**GK07**	**AS08**	**BA08**	**CB08**	**CY08**
PGA	0.98	0.91	1.12	0.92	1.41	1.12	0.93	1.42	2.82	0.94	0.61	0.63	0.77	0.53	0.61
SA (0.3s)	1.01	1.04	1.02	0.99	1.69	1.03	1.00	1.70	2.29	0.99	0.68	0.72	0.80	0.62	0.68
SA (1 s)	1.00	1.11	0.67	0.89	1.12	0.68	0.89	1.13	1.29	0.79	0.71	0.73	0.73	0.64	0.71
SA (3 s)	1.17	0.98	0.63	0.67	0.82	0.63	0.68	0.83	0.78	0.59	0.65	0.75	0.67	0.61	0.65

Table 2. Combined performance parameters of ground motion prediction equations (GMPEs; GMPE with the lowest performance parameter can be interpreted as better performing one (shown by bold).

M7.1 Darfield	**Combined Performance Parameter**				
	GK07	**AS08**	**BA08**	**CB08**	**CY08**
PGA	1.05	1.19	**1.04**	1.35	1.07
SA (0.3s)	**1.00**	1.16	1.04	1.24	1.09
SA (1 s)	1.07	1.07	**1.00**	1.06	1.11
SA (3 s)	**1.00**	1.18	1.19	1.28	1.35
M6.3 Christchurch	**Combined Performance Parameter**				
	GK07	**AS08**	**BA08**	**CB08**	**CY08**
PGA	1.17	1.08	1.37	2.36	**1.00**
SA (0.3s)	1.04	1.07	1.46	1.85	**1.00**
SA (1 s)	**1.01**	1.21	1.39	1.49	1.08
SA (3 s)	1.09	1.10	1.30	1.18	**1.02**